Journal of the Korean Physical Society, Vol. 65, No. 5, September 2014, pp. 664∼670

Structural, Mechanical and Magnetic Properties of Fe – 40-at.% Al Powders during Mechanical Alloying

Baris Avar*
Department of Metallurgical and Materials Engineering, Bulent Ecevit University, 67100 Zonguldak, Turkey

Musa Gogebakan
Department of Physics, Kahramanmaras Sutcu Imam University, 46100 Kahramanmaras, Turkey

Sadan Ozcan
Superconductivity and Nanotechnology Group, Department of Physics Engineering, Hacettepe University, 06800 Ankara, Turkey

Suleyman Kerli
Department of Energy Systems Engineering, Kahramanmaras Sutcu Imam University, 46300 Kahramanmaras, Turkey

(Received 28 April 2014, in final form 23 June 2014)

Nanocrystalline Fe – 40at.% Al alloy powders were prepared by using a mechanical alloying (MA) process with a planetary high-energy ball mill. The structural and the morphological properties of the powders were investigated by means of X-ray diffraction (XRD), and scanning electron microscopy (SEM), respectively. A disordered Fe(Al) solid solution with bcc crystal structure was formed after 10 h of MA. Longer MA durations introduced ordering in the alloyed powders. The final crystallite size was found to be as small as 5 nm whereas the internal strain was found to reach a final value of 2.1%. Also, the lattice parameter quickly increased to a maximum value of 0.2926 nm at 30 h of MA, and then decreased to a value of 0.2873 at 80 h of MA. SEM results showed variations in the shapes and the sizes of the particles in the powders at different stages. Furthermore, the microhardness values were found to increase gradually with increasing MA time due to work hardening, grain refinement and solid-solution formation. Magnetic properties such as the saturation magnetization (Ms) and the coercive field (Hc) were calculated from the hysteresis loops, and the results are presented as functions of the MA time.

PACS numbers: 61.66.Dk, 81.20.Ev
Keywords: Iron alloys, Nanocrystalline microstructure, Mechanical alloying, Hardness test, Magnetic properties
DOI: 10.3938/jkps.65.664

I. INTRODUCTION

Fe-Al alloys have generated considerable interest in the scienti?c community because of their unique properties: relatively high strength, high melting temperature, high electrical resistivity, excellent oxidation-corrosion resistance, low thermal conductivity, low density, low material cost compared to Ni-, Co-, and Fe-based superalloys, availability of raw materials, etc. These features have led to consideration of Fe-Al alloys for many structural, electrical, thermal, and magnetic applications [1–6]. Moreover, with the changes made in the chemical composition and microstructure in the Fe-Al alloys, different soft magnetic and physical properties can be obtained [7]. Experimental results have shown that Fe-Al alloys have a ferromagnetic, disordered, body-centered cubic (bcc) structure up to 22-at.% Al at room temperature and that the ferromagnetic state of the alloy decreases slowly with increasing Al content. At 30-at.% Al, the average magnetic moment per Fe atom decreases more rapidly and becomes zero. Above this Al concentration, the alloys are paramagnetic at room temperature, and the ordered bcc structure (B2) exists over the composition range 36- to 50-at.% Al. However, the atomically-ordered alloys at concentrations above 32-at.% Al can become ferromagnetic at room temperature, after having been disordered [8–10]. We note that the structural disorder (*e.g.*, internal stresses, grain boundaries, dislo-

*E-mail: barisavar@beun.edu.tr; Tel: +90-372-257-4010-1672; Fax: +90-372-257-4023

cations, and impurities) and lattice expansions have been found to increase the ferromagnetism (*e.g.*, increase the magnetic moment) [10].

By using mechanical alloying (MA) process, one can produce disordered Fe-Al solid-solution nanostructures. In this process, materials are produced in powder form, which can be compacted in to desired shapes with dimensions for the practical applications. This powder metallurgy process leads to an alloy formation by solid-state reactions assisted by the severe plastic deformation that occurs during MA of the elemental powders. The repeated stressing, deformation, fracturing, and cold welding of powder particles can lead to the formation of supersaturated solid solutions, nanocrystalline, quasicrystalline, and amorphous structures. The formation of these structures is well known to depend strongly the process conditions, such as the type of MA device, the MA time and temperature, the ball-to-powder weight ratio, the milling intensity, etc. However, even for the same nominal composition, different phases have been obtained by MA using the same type of MA device because MA is a complex multiparameter process [11–16].

In recent years, a number of studies have been reported on MA of Fe – 40-at.% Al. For instance, Wolski *et al.* [17] investigated the effect of milling conditions on the Fe – 40-at.% Al (Fe-40Al) intermetallic formed by MA. They reported that this process occurred in two steps, a nanocrystallization step and a FeAl formation step. Amils *et al.* [18] examined the changes in the hardness of the same alloy during MA and during subsequent annealing. In that work, the increase in hardness during MA was explained by the combined contributions of vacancy hardening, ordered domain/particle hardening, and disorder hardening within the ordered regions. Zeng and Baker [19] studied the effect of the MA time on the crystallite size, lattice strain, and lattice parameter of Fe-40Al powders. According to their results, a nanostructured disordered bcc Fe(Al) solid solution was formed after 2 h of MA. Increasing the MA time led to lattice expansion and a decreased paramagnetic fraction. Also, Nogues *et al.* [20] demonstrated experimentally and theoretically that about 35–45% of the magnetic moment of $Fe_{60}Al_{40}$ alloys arises from lattice expansion effects induced during the disordering process. Shokrollahi [21] reported that, generally, some magnetic properties could be enhanced when the grain size was reduced to nanoscale while the presence of stresses and defects introduced by MA impair the magnetic property. Zamora *et al.* [22] investigated the effect of MA time (12, 24 and 36 h) on the crystallite size, lattice parameter, and magnetic properties of $Fe_{1-x}Al_x$ alloys ($0.2 \leq x \leq 0.4$). According to their investigation, with increasing MA time, the lattice parameter remained constant, but the crystallite size increased. Also, they proposed a simple illustrative model to explain the occurrence of ferromagnetic behavior due to the presence of structural disorder. Besides these works, emphasis has mostly been on the magnetic properties and the order-disorder process during MA, without correlating them with structural and microhardness evolution. Thus, in the present work, mechanically-alloyed nanocrystalline Fe – 40-at.% Al powders were investigated by means of X-ray diffraction (XRD), scanning electron microscopy (SEM), Vickers microhardness (HV) testing, and vibrating sample magnetometry (VSM). The obtained results will be discussed in detail.

Table 1. Details of the MA conditions.

Rotation speed of disc (rpm)	300
Rotation speed of vial (rpm)	600
Vial material	Hardened steel
Capacity of vials (ml)	250
Diameter of the disc (mm)	250
Ball material	Hardened steel
Diameter of balls (mm)	10
Ball-to-powder weight ratio	10 : 1
Process control agent	1 wt.% stearic acid
Type of MA	Dry
Atmosphere	Argon
MA time (hour)	0 − 80

II. EXPERIMENTS

Pure Fe (99.9% purity, mean particle size < 10 μm) and Al (99.5% purity, mean particle size < 45 μm) elemental powders (both Merck products) were mechanically alloyed to produce a $Fe_{60}Al_{40}$ (at.%) alloy in a planetary-ball mill (Fritsch Pulverisette-5) at room temperature. The MA conditions are given in Table 1. Each 20 min of MA was followed by a pause of 20 min to avoid excessive heating during MA. The MA was interrupted at selected times, and a small amount of powder was removed for further characterization.

The structural evolution and the phase identification were investigated by using XRD with a Rigaku D-max/B diffractometer with Cu Kα radiation generated at 40 kV and 30 mA. The XRD analyses were performed at angles from 25 to 90° (2θ) with a step size of 0.02° and a count time of 1 s per step. The average crystallite size and lattice strain of the samples were calculated by using the following equations [11]:

$$D = \frac{0.9\lambda}{\beta \cos\theta}, \tag{1}$$

$$\varepsilon = \frac{\beta}{4 \tan\theta}, \tag{2}$$

where D is the crystallite size, ε is the lattice strain, λ is the wavelength of the X-ray radiation (0.15418 nm), θ

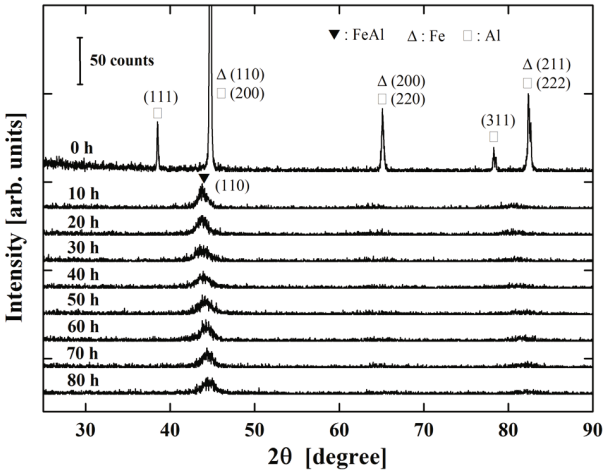

Fig. 1. XRD patterns of $Fe_{60}Al_{40}$ powders for various MA times.

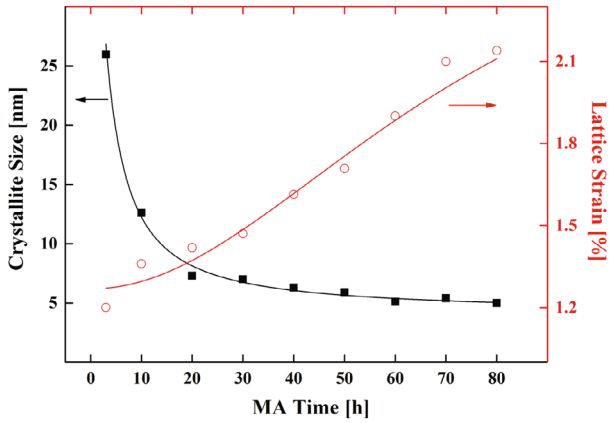

Fig. 2. (Color online) Crystallite size and lattice strain of $Fe_{60}Al_{40}$ powders as functions of MA time.

is the diffraction peak's position for the sample, and β is the full-width-at-half-maximum (FWHM). Instrumental broadening corrections were performed using an Y_2O_3 standard. Also, the pseudo-Voigt peak fitting function was used to fit the peak profile of the XRD pattern, and a polynomial function was used to determine the background. Lattice parameters of the samples were calculated using JADE software [23]. The morphology of the powder particles was characterized by SEM with a FEI-Quanta FEG 450 microscope at an acceleration voltage of 13 kV. The hardness of powders was also determined by microhardness test using a Vickers indenter. The Vickers microhardness (HV) tests were done at room temperature with a Shimadzu HMV-2 microhardness tester at a load of 100 g and a dwell time of 10 s. Five indentations were made on each sample to obtain an average value of the hardness. Prior to indentation, cross section of powder particles was prepared by mounting a small amount of powder in a resin, followed by conventional grinding and polishing. The magnetic properties were measured at 300 K in a maximum field of 20 kOe by using a superconducting quantum interference device (SQUID, Quantum Design MPMS7) equipped with a vibrating sample magnetometer.

III. RESULTS AND DISCUSSION

1. Structural Evolution

Figure 1 shows the XRD patterns of the $Fe_{60}Al_{40}$ powders as-received and after different MA times. The XRD spectrum for the as-received powders (labeled 0 h) shows reflections corresponding to distinct body-centered-cubic (bcc) Fe and face-centered-cubic (fcc) Al peaks, where Al (2 0 0), (2 2 0) and (2 2 2) peaks overlap with the Fe (1 1 0), (2 0 0) and (2 1 1) peaks, respectively. However, the diffraction peaks of Al (1 1 1) and (3 1 1) do not overlap. As seen, the first 10 h of the MA process led to the disappearance of these Fe and Al peaks, while resulting the presence of a single phase, a disordered Fe(Al) solid solution with a bcc crystal structure, where the peak corresponding to Fe(Al) (1 1 0) became the most intense one. This indicates that a solid solution had been formed because Al atoms, which have a larger atomic radius, dissolves into the Fe lattice. With increasing MA time, the diffraction peaks of the solid solutions were broadened and reduced in the intensity. This is due to the contribution of the crystallite size and to an increase in the atomic-level strain because of heavy plastic deformation [24]. Furthermore, during MA from 10 to 30 h, the Fe(Al) (1 1 0) peak shifted towards lower 2θ angles. This shift indicates that the Fe(Al) solid solution had been completely formed. A similar phase evolution was obtained for $Fe_{70}Al_{30}$ powders Kezrane *et al.* [25]. In their report, the bcc Fe(Al) solid solution was completely formed after 27 h of milling time. However, as can be seen in Fig. 1, with increasing MA time from 40 to 80 h, the angular position of the Fe(Al) (1 1 0) peak slightly shifted to a higher 2θ value, which signals ordering in the alloyed powders. This is in agreement with the results of Rajath Hegde *et al.* [26], wherein the Fe(Al) solid solution was transformed into an ordered FeAl phase after 28 h of milling in the case of $Fe_{50}Al_{50}$. According to Miedema's semi-empirical model for the Al-Fe system, an amorphous phase is predicted to form in the composition range from 25 to 60% Fe [5]. However, such an amorphous phase was not observed in the present study, probably because of the current experimental parameters (type of ball mill, the ball-to-powder ratio, the purity of the atmosphere during milling, *etc.*), which are likely to influence the range over which the amorphous phase occurs.

As mentioned above, the change in the XRD peak's broadening is associated with both crystallite size refinement and increased lattice strain. The crystallite size

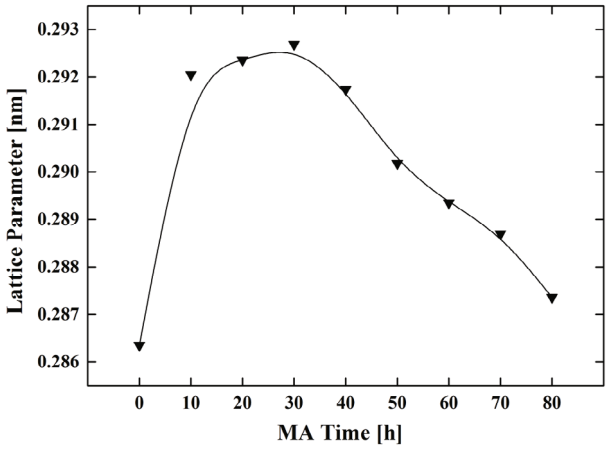

Fig. 3. Variations of the lattice parameter of $Fe_{60}Al_{40}$ powders with the MA time.

and the lattice strain of the major phase were calculated from the broadening of the XRD peaks by using Eqs. (1) and (2), after correcting for instrumental broadening. Figure 2 shows the evolution of the crystallite sizes (D) and the level of internal strains (ε) along (1 1 0) direction as functions of MA time. Clearly, the reduction in crystallite size is accompanied by an increase in the lattice strain level as the MA time increases. This is a common behavior for all metallic systems prepared by MA [21]. As can be seen in Fig. 2, the crystallite size decreased rapidly to about 7.3 nm in the early stage of MA (at 20 h) and the rate of decrease slowed down afterwards. After 30 h of MA, the crystallite size became gradually smaller with increasing MA time, with a final value of about 5 nm. The internal strain increased steadily with increasing MA time and reached a final value of 2.1%, as seen in Fig. 2. Similar values were reported by Mhadhbi *et al.* [24] for the same composition. We note that, during the course of the MA process, severe plastic deformation leads to an increasing number of matrix dislocations. The successive accumulation and interaction of dislocations cause a reduction in the crystallite size and an increase in the lattice strain [27].

Figure 3 shows the lattice parameter (a) as a function of the MA time for $Fe_{60}Al_{40}$ powders. The Fe and Fe(Al) lattice parameters were calculated, with accuracy of 0.02%, from the shift of their diffraction (1 1 0) peak's position. As one can see, during the first 10 h of MA, the lattice parameter monotonously increased from 0.2863 nm for pure Fe (0 h) to 0.2920 nm. When the MA was continued to 30 h, the lattice parameter increased slightly to reach a steady value of 0.2926 nm. This can be attributed to substitutional dissolution of Al in the Fe lattice, because the atomic radius of Al (0.142 nm) is larger than that of Fe (0.123 nm) [7,15,26]. Another reason for the increase in the lattice parameter is probably the lattice expansion due to the increase in the density of dislocations, with their characteristic strain fields, on the nanograin boundary [6,24,25]. After 30 h of MA, the lattice parameter decreased monotonously with increasing MA time and reached a final value of 0.2873 nm. Such a decrease in the lattice parameter of Fe-Al powders was observed by Hamlati *et al.* [15,28] and was attributed to the ordered structure.

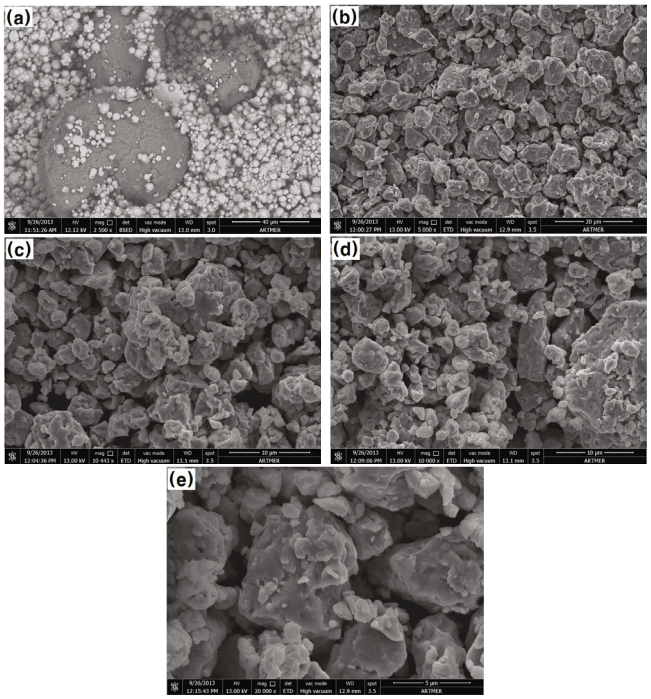

Fig. 4. SEM micrographs of $Fe_{60}Al_{40}$ powders for various MA times: (a) 0, (b) 10, (c) 30, (d) 50 and (e) 80 h.

2. Morphological Changes

The morphologies of $Fe_{60}Al_{40}$ powders as-received and after various MA times are shown in Fig. 4. Clearly, different morphologies are present during the MA. For the as-received powders (0 h), smaller particles of Fe (light color) and larger ones of Al (gray color) are clearly observed (Fig. 4(a)). When the MA time is 10 h, all the initial shapes of the powders were changed, and new surfaces were formed with sizes ranging between 1 μm and 6 μm (Fig. 4(b)). Also, the powder's particles were found to be irregular in shape and to be flattened because of the strong plastic deformation that was accompanied by particle fracture [24]. For extended MA (30 h and 50 h), the morphology became inhomogeneous because of the cold welding of the small particles to the surfaces of large ones. Figures 4(c) and (d) show the lamellar, and roughly-spherical agglomerate particles within the range of about $2 - 7$ μm. Longer MA times (> 80 h) led to a matrix of randomly-welded thin layers of highly-deformed particles. This layered structure was produced due to cold welding and repeated mechanical deformations [24, 29]. Also, the particle sizes were in the range

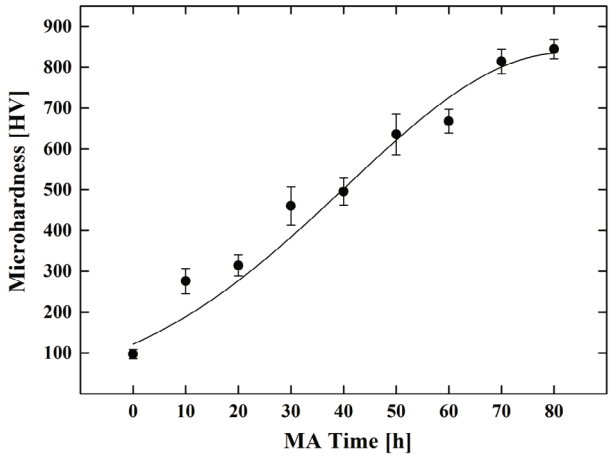

Fig. 5. Microhardness values of $Fe_{60}Al_{40}$ powders as a function of MA time.

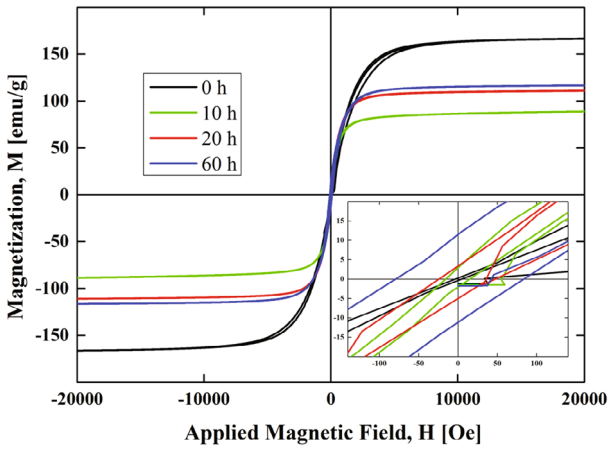

Fig. 6. (Color online) Hysteresis loops of the powders at different MA times.

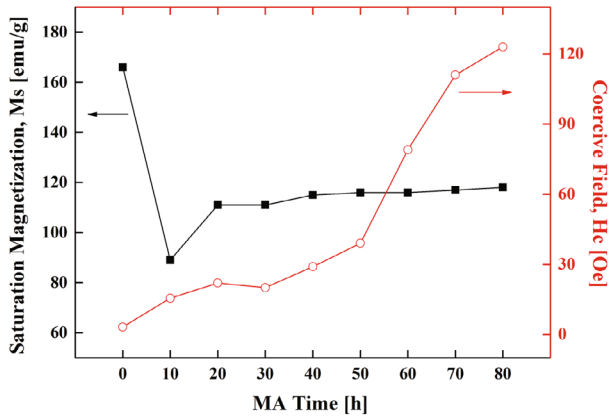

Fig. 7. Variation of Ms and Hc with the MA time.

of 200 nm − 6 μm (Fig. 4(e)).

3. Microhardness Measurements

Figure 5 shows the average Vickers microhardness (HV) values (with standard deviations from 5 measurements) of the $Fe_{60}Al_{40}$ powders at different MA times. As can be seen, increasing the MA time for the starting powders enhanced the hardness of the powders. The increasing microhardness during MA may be attributed to several effects including work hardening, grain refinement and solid-solution formation [30]. Besides these effects, a disorder-to-order transition is another cause of the enhanced hardness after 40 h of MA [26]. This is due to lattice contraction (Fig. 3). The maximum microhardness value was found to be 845 ± 24 $HV_{0.1}$ (8.29 ± 0.23 GPa) for 80 h of MA. This value is slightly higher than the reported values for $Fe_{50}Al_{50}$ [26] and $Fe_{75}Al_{25}$ [30] powders prepared by using the same procedure, probably due to a refinement of the grain size. Moreover, the microhardness of a nanocrystalline FeAl intermetallic prepared by using MA and hot forging was found to be 680 $HV_{0.3}$ [31], as reported in Refs. [2], [32], and [33], while that of the $Fe_{50}Al_{50}$ mechanically alloyed for 80 h and subsequently sintered for 3 h at 800 − 1100 °C was in the range of 337 − 453 $HV_{0.1}$ [34]. The maximum hardness in this work is significantly higher than those reported values, probably due to the elimination of both lattice defects and internal strain during annealing.

4. Magnetic Studies

Figure 6 shows the hysteresis loops (magnetization M versus applied magnetic field H) for selected samples of $Fe_{60}Al_{40}$ powders (0, 10, 20 and 60 h) by applying an external field between −2 and +2 T at 300 K. All the alloy powders exhibited similar hysteresis loops, typical of a ferromagnetic state. The saturation magnetization (Ms) and the coercive field (Hc) were obtained from these hysteresis loops, and Fig. 7 illustrates Ms and Hc as functions of the MA time. From this figure, one can see that during the initial stage of the MA process (up to 10 h), the Ms rapidly decreased from a value of 166 emu/g, attained a minimum value of 89 emu/g, and then slightly increased and remained nearly constant on further MA. Meanwhile, the Hc gradually increased with increasing MA time and reached a maximum value of about 120 Oe at 80 h of MA. The rapid decrease in Ms is mainly due to the dilution of the magnetic lattice of Fe caused by Al, as evidenced by the XRD analysis (increasing lattice parameter). Al has been reported to decrease the magnetic moment of individual Fe sites due to a decrease in the direct ferromagnetic interaction between Fe-Fe sites and to an antiferromagnetic superexchange interaction between Fe sites mediated by Al atoms [9,16,19,35]. After 10 h of MA, the slight increase in Ms of the aggregates can be attributed to the formation of a solid solution of Fe(Al) and a diminution of the magnetocrystalline anisotropy

due to the grain refinement, which leads to an easier rotation of the magnetic vectors [36]. However, according to the Refs. 9 and 19, such an increase in Ms can be ascribed to Fe contamination from the milling media and to oxidation of Al, which causes a decreasing in the Al content. On prolonged MA, the Ms was not increased distinctly because the crystallite size was nearly constant. A similar behavior was observed for $Fe_{50}Al_{30}Cu_{20}$ powders [16]. In addition, the increase in Hc during the MA process can be attributed to the progressive formation of the solid solution and to a decrease in the crystallite size, which is associated with an increase in the stresses during MA. This effect has been reported previously as the internal stress can be the prevailing factor in the coercivity, which leads to an increase in the Hc with increasing MA time rather than to the usual effect of a crystallite-size reduction [37]. Indeed, the internal stress may ensure a narrow and irregular type of magnetic domain, which could increase the Hc significantly. The sample could be annealed at a suitable temperature in order to reduce the Hc. This would eliminate the irregular domain patterns and reduce the coercivity, leading to larger crystallite sizes [38]. Another reason for the increase in the Hc might be the high levels of impurities and various defects (dislocations). During MA, impurities like inclusions and oxides could be introduced to the powders from the vial, the balls, or the atmosphere of the vial. Those impurities or nonmagnetic inclusions could increase the Hc by pinning the magnetic domain walls [39].

IV. CONCLUSION

The outcome of this study can be summarized as follows:

1. The MA process was successfully applied to the synthesis of a nanocrystalline bcc Fe(Al) solid solution.

2. After 10 h of MA, the dissolution of Al in the Fe lattice led to the formation of a disordered Fe(Al) solid solution with a bcc crystal structure. Longer MA durations introduced ordering in the alloyed powders.

3. Increasing the MA time led to increases in the values of the lattice parameter and the strain values, but to a decrease in the crystallite size. Typically, these values were estimated to be around 0.2873 nm, 2.1% and 5 nm, respectively, for the 80-h mechanically-alloyed powders.

4. SEM results revealed that small particles were cold-welded to the surfaces of large ones and that the powder's particles tended to form a matrix of randomly-welded thin layers of highly-deformed particles.

5. The increase in microhardness during the MA process is due to work hardening, grain refinement and solid-solution formation. Besides these effects, a disorder-to-order transition can also enhance the hardness value.

6. The Ms was found to rapidly decrease in the first stage of MA due to the magnetic dilution caused by the Al. As the MA process was continued, the Ms slightly increased due to solid-solution formation and reduction in the magnetocrystalline anisotropy caused by the grain refinement. Meanwhile, the Hc increased with increasing MA time, where the internal stress may be the dominating factor in the coercivity rather than the usual effect of crystallite size reduction. Also, the introduction of impurities and various defects (dislocations) may increase the Hc during the course of the MA process.

ACKNOWLEDGMENTS

The author (B. Avar) would like to thank the TUBITAK-BIDEP 2218 National Research Fellowship Programme.

REFERENCES

[1] E. P. George and I. Baker, *The Encyclopedia of Materials: Science and Technology* (Elsevier Press, Oxford, 2001), p. 4201.
[2] L. D'Angelo, L. D'Onofrio and G. Gonzalez, J. Alloys Comp. **483**, 154 (2009)
[3] H. Wu, I. Baker, Y. Liu, X. Wu and J. Cheng, Intermetallics **19**, 1517 (2011).
[4] M. Mhadhbi, M. Khitouni, L. Escoda, J. J. Sunol and M. Dammak, J. Alloys Comp. **509**, 3293 (2011).
[5] F. Hadef, A. Otmani, A. Djekoun and J. M. Greneche, J. Magn. Magn. Mater. **326**, 261 (2013).
[6] M. Krifa, M. Mhadhbi, L. Escoda, J. M. Guell, J. J. Sunol, N. Llorca-Isern, C. Artieda-Guzman and M. Khitouni, J. Alloys Comp. **554**, 51 (2013).
[7] N. Boukherroub, A. Guittoum, N. Souami, K. Akkouche and S. Boutarfaia, EPJ Web Conf. **29**, 00010 (2012).
[8] E. Menendez, J. Sort, M. O. Liedke, J. Fassbender, S. Surinach, M. D. Baro and J. Nogues, New J. Phys. **10**, 103030 (2008).
[9] R. Bernal-Correa, A. Rosales-Rivera, P. Pineda-Gomez and N. A. Salazar, J. Alloys Comp. **495**, 491 (2010).
[10] Y. Jiraskova, J. Bursik, J. Cizek and D. Jancik, J. Alloys Comp. **568**, 106 (2013).
[11] C. Suryanarayana, *Mechanical Alloying and Milling* (Marcel Dekker, New York, 2004).
[12] M. Gogebakan and B. Avar, Mater. Sci. Tech. **26**, 920 (2010).
[13] M. Gogebakan and B. Avar, Pramana J. Phys. **77**, 735 (2011).

[14] F. Hadef, A. Otmani, A. Djekoun and J. M. Greneche, Super Microstruct. **49**, 654 (2011).
[15] Z. Hamlati, A. Guittoum, S. Bergheul, N. Souami, K. Taibi and M. Azzaz, J. Mater. Eng. Perform. **21**, 1943 (2012).
[16] M. Krifa, M. Mhadhbi, L. Escoda, J. M. Guell, J. J. Sunol, N. Llorca-Isern, C. Artieda-Guzman and M. Khitouni, Powder Tech. **246**, 117 (2013).
[17] K. Wolski, G. Le Caer, P. Delcroix, R. Fillit, F. Thevenot and J. Le Coze, Mater. Sci. Eng. A **207**, 97 (1996).
[18] X. Amils, J. Nogues, S. Surinach, M. D. Baro, M. A. Munoz-Morris and D. G. Morris, Intermetallics **8**, 805 (2000).
[19] Q. Zeng, I. Baker, Intermetallics **14**, 396 (2006).
[20] J. Nogues *et al.*, Phys. Rev. B **74**, 024407 (2006).
[21] H. Shokrollahi, Mater. Des. **30**, 3374 (2009).
[22] L. E. Zamora, G. A. P. Alcazar, G. Y. Velez, J. D. Betancur, J. F. Marco, J. J. Romero, A. Martinez, F. J. Palomares and J. M. Gonzalez, Phys. Rev. B **79**, 094418 (2009).
[23] MDI Jade Software, XRD pattern processing, Material Data Inc. Livermare CA, USA.
[24] M. Mhadhbi, M. Khitouni, L. Escoda, J. J. Sunol and M. Dammak, J. Nanomater. **2010**, 712407 (2010).
[25] M. Kezrane, A. Guittoumb, N. Boukherroubc, S. Lamranic and T. Sahraoui, J. Alloys Comp. **536S**, 304 (2012).
[26] M. M. Rajath Hegde and A. O. Surendranathan, Powder Metall. Metal Ceram. **48**, 641 (2009).
[27] M. H. Enayati, G. R. Aryanpour and A. Ebnonnasir, Int. J. Ref. Met. Hard. Mater. **27**, 159 (2009).
[28] Z. Hamlati, A. Guittoum, S. Bergheul, N. Souami, K. Taibi and M. Azzaz, Adv. Mater. Res. **214**, 490 (2011).
[29] M. Khajepour and S. Sharafi, Powder Tech. **232**, 124 (2012).
[30] M. Rafiei, M. H. Enayati and F. Karimzadeh, J. Mater. Sci. **45**, 4058 (2010).
[31] M. A. Morris-Munoz, A. Dodge and D. G. Morris, Nanostruct. Mater. **11**, 873 (1999).
[32] M. Krasnowski and T. Kulik, Intermetallics **15**, 201 (2007).
[33] B. Song, S. Dong, P. Coddet, H. Liao and C. Coddet, Surf. Coat. Technol. **206**, 4704 (2012).
[34] S. Izadi, G. H. Akbari and K. Janghorban, J. Alloys Comp. **496**, 699 (2010).
[35] J. A. Plascak, L. E. Zamora and G. A. P. Alcazar, Phys. Rev. B **61**, 3188 (2000).
[36] N. Bensebaa, N. Loudjani, S. Alleg, L. Dekhil, J. J. Sunol, M. Al Sae and M. Bououdina, J. Magn. Magn. Mater. **349**, 51 (2014).
[37] A. Guittoum, A. Layadi, A. Bourzami, H. Tafat, N. Souami, S. Boutarfaia and D. Lacour, J. Magn. Magn. Mater. **320**, 1385 (2008).
[38] A. H. Bahrami, H. Ghayour and S. Sharafi, Powder Tech. **249**, 7 (2013).
[39] A. Sharifati, S. Sharafi, Mater. Des. **41**, 8 (2012).